Astron. Astrophys. 348, 924–932 (1999)

ASTRONOMY AND ASTROPHYSICS

Multi element Doppler imaging of Ap stars

I. He, Mg, Si, Cr and Fe surface distribution for CU Virginis⋆

R. Kuschnig[1], **T.A. Ryabchikova**[2], **N.E. Piskunov**[3], **W.W. Weiss**[1], **and M.J. Gelbmann**[1]

[1] Institute of Astronomy, University Vienna, Türkenschanzstrasse 17, A-1180 Vienna, Austria (last_name@galileo.astro.univie.ac.at)
[2] Institute of Astronomy, Russian Academy of Sciences, Pyatnitskaya 48, 109017 Moscow, Russia (ryabchik@inasan.rssi.ru)
[3] Uppsala Astronomical Observatory, Box 515, S-751 20, Uppsala, Sweden (piskunov@astro.uu.se)

Received 2 February 1999 / Accepted 16 June 1999

Abstract. We present the distribution of helium, magnesium, silicon, chromium and iron on the surface of the fast rotating magnetic B9p Si star CU Virginis, obtained with a Doppler Imaging inversion code. A clearly defined helium spot coincides with the position of one magnetic pole whereas silicon, chromium and iron accumulate in regions where the magnetic field lines are dominantly horizontal in the stellar atmosphere. The distribution of magnesium is significantly different compared to the other elements. The Hδ line varies in phase with the helium spot and the magnetic pole and the line profiles can be fitted within the observational errors with model atmospheres of constant $T_{\rm eff}$ of 12500 K, but different surface gravity.

We compare our observations with current concepts for diffusion in magnetic chemically peculiar stars and find good agreement.

Key words: methods: data analysis – stars: abundances – stars: chemically peculiar – stars: individual: CU Vir – stars: magnetic fields

1. Introduction

Doppler Imaging is a technique which inverts rotationally modulated spectral line profiles to a surface abundance distribution, a so called Doppler map. History, principles and applications of Doppler Imaging techniques were comprehensively reviewed by Rice (1996) and Hatzes (1996). Doppler Imaging was first applied to magnetic Ap (CP2) stars (Preston 1974), because many of these stars show strong changes of their spectral line profiles and the magnetic field due to rotation in accordance with the oblique rotator model (Stibbs 1950). The structure of magnetic Ap stars is believed to be basically constant everywhere in the atmosphere so that line profile variations should be mainly due to surface abundance inhomogeneities. Presently, the most successful theory in explaining the chemical peculiarities of these stars is based on radiative diffusion of elements in the atmosphere (Michaud 1970) which is influenced by the orientation and strength of a local magnetic field. This effect was studied particularly for silicon by Michaud et al. (1981), Megessier (1984) and Vauclair et al. (1991).

CU Vir is a well studied B9p Si star (HD 124224, HR 5313, V = 5.01 mag). It is a photometric, spectrum and magnetic variable with one of the shortest known rotational periods among Ap stars. Weiss et al. (1976) found $H\beta$ variations in anti-phase to the light curve, indicating considerable atmospheric inhomogeneities also in $T_{\rm eff}$ and $\log\ g$ which were discussed in detail by Musielok & Madej (1988). Silicon Doppler maps of CU Vir based on different inversion techniques and observations were published by Goncharski et al. (1983) and Hatzes (1993, 1996, 1997). Hiesberger et al. (1995) produced the first Helium map using a Doppler Imaging code which is described in detail by Piskunov & Rice (1993), and further elements were mapped in Kuschnig et al. (1996).

A recent study (Pyper et al. 1998) was focused on the stability of the rotation period of this very fast rotating Ap star and led to convincing evidence for a significant period change around the year 1985 from $0\overset{\rm d}{.}5206778$ to $0\overset{\rm d}{.}5207031 \pm 0.00000019$, perhaps due to an interaction of rotation with the global magnetic field (Stepien 1998). The evidence is based on more than 30 independent photometric, spectroscopic and magnetic field data sets obtained during the last 4 decades, including also the equivalent widths measurements presented in this paper. An observing programme is being continued in order to confirm this new and outstanding result, which seems to be unique for an otherwise "normal" star. The ephemeris used for the present Doppler mapping is adopted from Pyper et al. (1998).

2. Observations and data reduction

The observations were obtained in June, 1994, and in March, 1995, at the Observatoire d'Haute-Provence using the spectrograph AURELIE in two spectral regions: 4060–4260 Å (1995 observing run) and 4440 – 4640 Å (data from 1994 and a few additional phases from 1995). The spectral resolution is about 20000 and a signal–to–noise ratio of better than 150 was achieved for all the spectra. The data reduction, wavelength calibration and normalization was performed with the PCIPS soft-

Send offprint requests to: Rainer Kuschnig (kuschnig@geop.ubc.ca)

⋆ Based on observation obtained at the Observatoire d'Haute-Provence

Table 1. Observing log and equivalent widths for Hδ and Si ii. The lines and spectral ranges are given in Table 4. Phases are given for JD = 2435178.$^{\rm d}$9025 + 0.$^{\rm d}$52070308·E.

	4060–4260 Å		
JD 2449000+	phase	Hδ	Si ii 4128-30 Å
798.489	0.628	10.230	0.626
798.622	0.883	9.537	0.942
799.434	0.443	9.344	0.409
799.575	0.713	10.025	0.766
799.612	0.784	9.839	0.879
800.410	0.317	9.402	0.611
800.502	0.494	10.018	0.424
800.599	0.680	10.193	0.738
801.412	0.241	8.594	0.569
802.415	0.167	9.050	0.785
803.438	0.132	8.863	0.772
804.444	0.064	9.061	0.887
804.468	0.110	9.063	0.875
806.413	0.846	9.605	0.925
806.435	0.888	9.483	0.952
806.452	0.920	9.358	0.950
806.469	0.953	9.218	0.906
806.484	0.982	9.212	0.903
806.500	0.013	9.154	0.894

Table 2. Observing log and equivalent widths for He i and Fe ii. The lines and spectral ranges are given in Table 4. Phases are given for JD = 2435178.$^{\rm d}$9025 + 0.$^{\rm d}$52070308·E.

	4450–4650 Å		
JD 2449000+	phase	He i 4471 Å	Fe ii 4520-22 Å
513.431	0.179	0.207	0.307
510.357	0.276	0.223	0.253
510.377	0.314	0.250	0.256
510.402	0.362	0.283	0.221
510.417	0.391	0.317	0.221
510.461	0.476	0.363	0.164
510.481	0.514	0.385	0.149
510.527	0.602	0.366	0.149
519.396	0.635	0.364	0.172
801.620	0.641	0.364	0.212
510.563	0.671	0.321	0.239
510.594	0.731	0.255	0.264
516.344	0.774	0.182	0.224
510.652	0.842	0.175	0.241
517.423	0.846	0.192	0.240
797.561	0.845	0.145	0.296
799.666	0.888	0.141	0.266
513.360	0.043	0.210	0.296
516.508	0.089	0.213	0.283

ware (Smirnov & Piskunov 1994). Tables 1 and 2 summarize the observations obtained in the two wavelength regions.

3. Equivalent width variations

The variations of the Hδ line equivalent widths and lines we used for mapping (listed in Table 4) are illustrated in Fig. 1. The Hδ equivalent width changes are significant and vary slightly out of phase with helium. The magnesium variation is very weak, whereas silicon, chromium and iron vary strongly, but in antiphase to Hδ and helium. In particular silicon line equivalent widths are correlated with the Johnson B-magnitudes in the sense that light minimum coincides exactly with the minimum of the Si ii lines intensity. We will comment more on the hydrogen line variations in Sect. 5.4.

4. Doppler imaging

The significance of Doppler Imaging for chemically peculiar stars is to provide observational constrains for the diffusion mechanism in the presence of radiation and a global magnetic field. Models which predict certain ions to rise, sink or move horizontally in the stellar atmosphere need to by verified. The few Ap stars with reliable Doppler maps did not allow to draw statistically sound conclusions. A further shortcoming of earlier studies was the limited number of elements mapped, mostly Si and occasionally Fe or Cr. Hence, it was difficult to disentangle effects due to an insufficient knowledge of the atomic parameters for a given element from incorrectly modeled atmospheric and magnetic field structures. As the diffusion process in magnetic Ap stars depends strongly on the electronic configuration of a given ion, simultaneous mapping of as many different species as possible helps to constrain significantly the number of free model parameters. All this considered, we embarked on a program for *multi-element Doppler Imaging* with the aim to map a statistically significant sample of stars.

Table 3. The final model atmosphere parameters for CU Vir, the range and stepsize for the grid of models investigated.

parameter	final	range	Δ
$T_{\rm eff}$	13000 K	12000–14000 K	500 K
$\log\ g$	4.0	3.8–4.2	0.2
$v \cdot \sin i$	160 km s^{-1}	140–180 km s^{-1}	10 km s^{-1}
i	30°	20–80°	10°

4.1. Input parameters

The starting values in our analysis of CU Vir for $T_{\rm eff}$, $\log\ g$, $v \cdot \sin i$ and the inclination angle i were taken from the literature (Hatzes 1993, Hiesberger et al. 1995), but a larger parameter space was checked in order to choose the proper model atmosphere for mapping (see Table 3). Finally, more than 120 maps were calculated to determine the parameter combination which minimizes the residuals between observations and the synthesized line profiles. We found the best inversion results with a Kurucz (1993) ATLAS 9 model atmosphere using $T_{\rm eff}$ = 13000 K and $\log\ g$ = 4.0, assuming the following stellar parameters: $v \cdot \sin i$ = 160 km s^{-1}, and i = 30°. A total of 19 phases were available for the surface mapping in each spectral region.

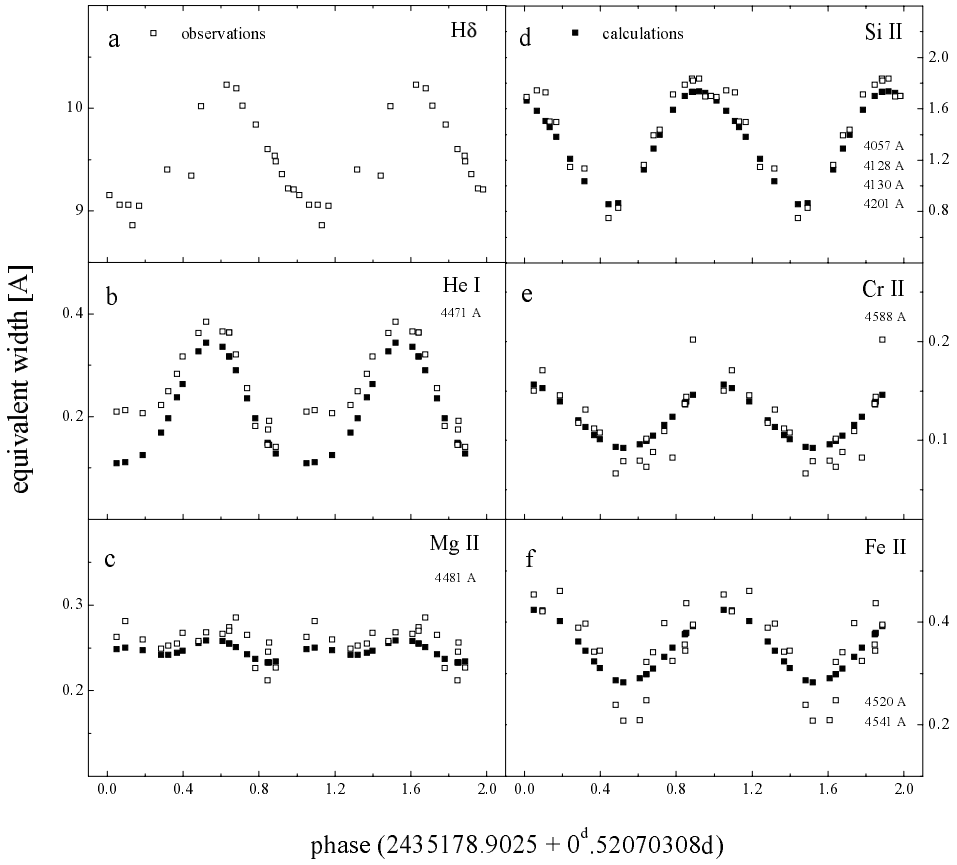

Fig. 1. Equivalent width variations for CU Vir. Open squares refer to individual spectra, filled squares are obtained from the line profiles derived from the final map. Phase Φ for JD=2435178.$^{\rm d}$9025 + 0.$^{\rm d}$52070308 E. For Si *ii* we show the sum of equivalent widths of the four listed lines.

The atomic line data required to compute the local line profile tables were extracted from VALD (Piskunov et al. 1995) and a grid of 40 steps in latitude and 80 in longitude was chosen for the inversion which is consistent with the rotational velocity and spectral resolution. Based on the recent determination of the rotation period of CU Vir (Pyper et al. 1998) we used the following ephemeris:

$$\mathrm{JD(U,B)_{maxlight}} = 2435178.^{\rm d}9025 + 0.^{\rm d}52070308 \cdot E$$

4.2. The maps and figures

The characteristics of the Doppler images obtained for He, Mg, Si, Cr and Fe are described in the following subsections, ordered by the atomic weights and are illustrated in Figs. 2 to 6. Each figure consists of three panels:

- *a:* is the mercator projection of the abundance distribution, longitude zero refers to phase zero. Because of an inclination angle of 30° the mercator projection gives relevant abundances only for latitudes higher than -15°.
- *b:* shows the abundance distribution in spherical projection for four characteristic phases.
- *c:* compares observed (crosses) and calculated (solid lines) line profiles. Phase zero is on the top and the vertical offsets are proportional to the respective rotation phases which are given on the right hand side of each spectrum. On the bottom the number of iterations needed (Niter) is listed and the mean difference (Devi) per wavelength bin in% between observation and synthesis.

Table 4. The elements (column 1), spectral range (column 2), and central wavelengths of the atomic lines (column 3) used for our inversion procedure. The figures in brackets in column 3 are the number of individual lines contributing to each blend.

element	range (Å)	lines (Å)
He	4464.0–4478.0	He I: 4471(6)
Mg	4478.0–4485.0	Mg II: 4481(3)
Si	4054.0–4060.0	Si II: 4057(2)
	4125.0–4135.0	Si II: 4128, 4130(2)
	4194.0–4205.0	Si II: 4198, 4200(2)
Cr	4586.0–4594.0	Cr II: 4587, 4588(2)
		Cr II: 4589 (6), 4592
Fe	4511.0–4527.0	Fe II: 4512(3), 4515(2)
		Fe II: 4520, 4522, 4524
		Fe II: 4525, 4526(2)
	4538.5–4544.5	Fe II: 4541(2), 4545

A definite problem in visualizing data and results is the proper choice of graphics lay-out and scaling factors. After some internal discussions which culminated in a "beauty competition" we selected the design and parameter values used for the present paper. We had, however, to accept a problem with Fig. 5 and less so with Fig. 6 where panels "*c:*" barely show line profile varia-

tions, because the scale factors in x and y were chosen to be the same for all maps in this paper. A comparison of our synthetic equivalent width variations with the actual observations (Fig. 1), however, illustrates the information content useable for Doppler imaging even of shallow lines in the spectrum of CU Vir. The contrast in the Cr lines region is poor for the given scale factors due to heavy blending, but this wavelength range was chosen such to include only blends of the same element (see Table 4) which allows to deduce consisten results.

4.2.1. Helium

The helium map shown in Fig. 2 was obtained from the group of lines at λ 4471 Å which consists of six helium blends (Table 4), but the red wing of this blend itself is significantly blended by an iron line, which explains rather large deviations for the fits. Also the systematically lower equivalent widths of the calculated line profiles compared to the observed ones are explained by this iron blend (Fig. 2d, open symbols). However, the He abundance variations are so strong that they dominate all effects from blends of other elements.

A strong He spot is present at about 200° longitude, +30° latitude, and with a diameter of about 40° and which seems to coincide with a magnetic pole (see our discussion in Sect. 5.3). Another but low contrast feature is visible at $l = 20°$ close to the stellar equator. On average, helium is strongly depleted (-1.05 dex) relative to the sun, except in the core of the spot.

Our analysis is in excellent agreement with the results published by Hiesberger et al. (1995) after the phases were corrected according to the ephemeris proposed by Pyper et al. (1998).

4.2.2. Magnesium

The surface distribution of magnesium is shown in Fig. 3. The significant line profile changes of the strong Mg ii 4481 Å blend contrast to the extremely low amplitude variations of the equivalent widths plotted in Fig. 3d. The resulting element distribution is characterized by a ring-like feature centered on $l = 200°$ and $b = 30°$ with a diameter of about 50°. In addition, a low contrast structure extends from $l = 340°$ to $l = 100°$. The average Mg abundance is about 1.5 dex lower than the solar value.

4.2.3. Silicon

For the determination of the silicon distribution three different Si blends were mapped separately in a first step and a second time simultaneously for the final result (see Table 4). It ought to be mentioned that Si ii 4057 Å and 4201 Å are much weaker lines compared to the popular 4128–4130 Å blend. The resulting silicon distribution (Fig. 4) indicates a depletion region from $l = 90°$ to $l = 250°$ which extends from below the southern horizon to about $b = +50°$ where the abundance drops below -6.0 dex (-4.49 for the sun). The rest of the sphere shows an average Si enhancement by about 1.2 dex.

Our map is based on six different lines in three different spectral regions. Despite of this complication our fit is good and the calculated equivalent widths reproduce the observations very well.

4.2.4. Chromium

The Cr distribution (Fig. 5) is based on 9 different Cr ii lines in the region from 4586 Å to 4594 Å. A depleted area at $l = 200°$ and $b = 20°$ is clearly present with about 40° in diameter. Outside this region chromium appears to be enhanced by about 0.6 dex compared to the sun. Furthermore, a region where the Cr abundance is more than 10 times higher than for the sun can be found between $l = 320°$ and $l = 60°$ (near phase zero). The latitude of this feature ranges from 5° to 65°.

4.2.5. Iron

For the iron map presented in Fig. 6 lines in two neighboring spectral regions were analyzed simultaneously and are listed in Table 4. An underabundant spot resolved with high contrast is centered at $l = 200°$, $b = 30°$ and with about 50° in diameter. At phase zero the mean iron abundance is about 0.3 dex higher than for the sun and in the central area of the depleted spot the abundance drops below -6.0 dex, which reflects the strong decrease in equivalent widths of the Fe lines at phases around 0.5 (see Fig. 6c).

5. Discussion

5.1. Surface distribution of elements

Comparing the abundance maps of all five elements presented in this paper, the most conspicuous result is the strong helium spot ($l = 200°$, $b = +30°$, $d = 40°$) which coincides with the position of silicon, chromium and iron depletion. This situation is also reflected in the equivalent width variations shown in Fig. 1. The only element which does not follow this pattern is magnesium. The Mg map (Fig. 3), which presents the first stellar surface distribution of that element published for an Ap star, shows that the most prominent magnesium feature is a ring-like structure centered on the He spot. Furthermore, the disk-averaged abundance variations plotted in Fig. 7 illustrate the differences in the behaviour of the five elements in the atmosphere of CU Virginis. Helium is globally depleted with respect to the sun except for the center of the helium spot. Magnesium in general is also underabundant by a factor of 30, although its distribution is more complex and the disk average abundance changes only marginally with the rotation phase. Silicon, chromium and iron are enhanced compared to the sun except in the helium spot. The highest overabundance is found for silicon (factor of 12) followed by chromium (about 10 times) and iron (3.5 times the solar value).

A comparison of our results with the published maps is not straightforward due to the fact that the rotation period seems to have changed, as was mentioned above. Nevertheless, the high contrast helium spot is also described in Hiesberger et al. (1995) based on observations obtained in 1982 with a totally different instrumentation. Although the phase coverage and the signal–

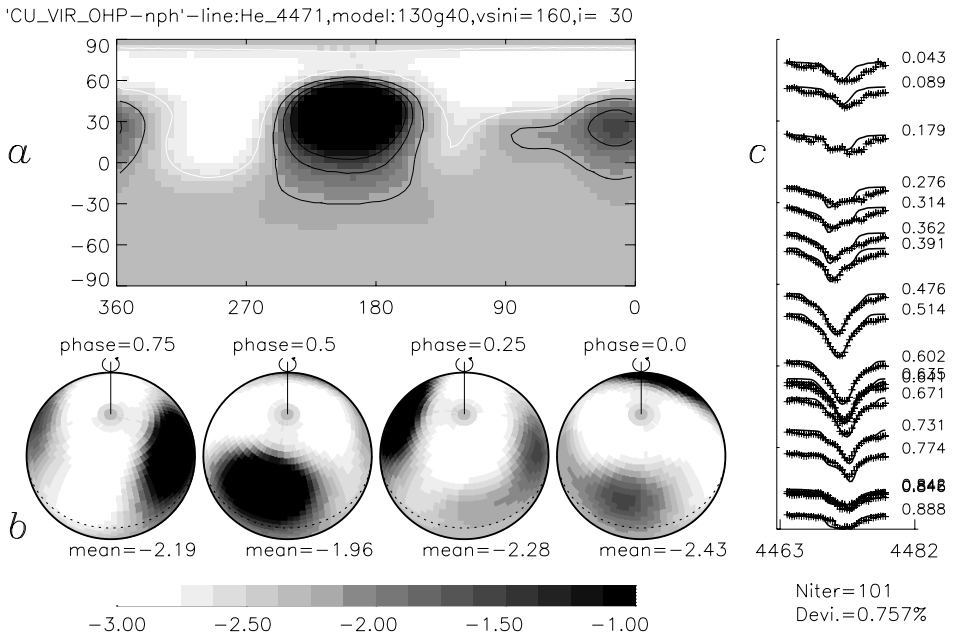

Fig. 2a–c. The helium map of CU Vir derived from the lines at 4471 Å, in mercator projection **a** and spherical projection **b**. The comparison of the line profiles is shown in **c** with crosses (observations) and solid lines (calculations).

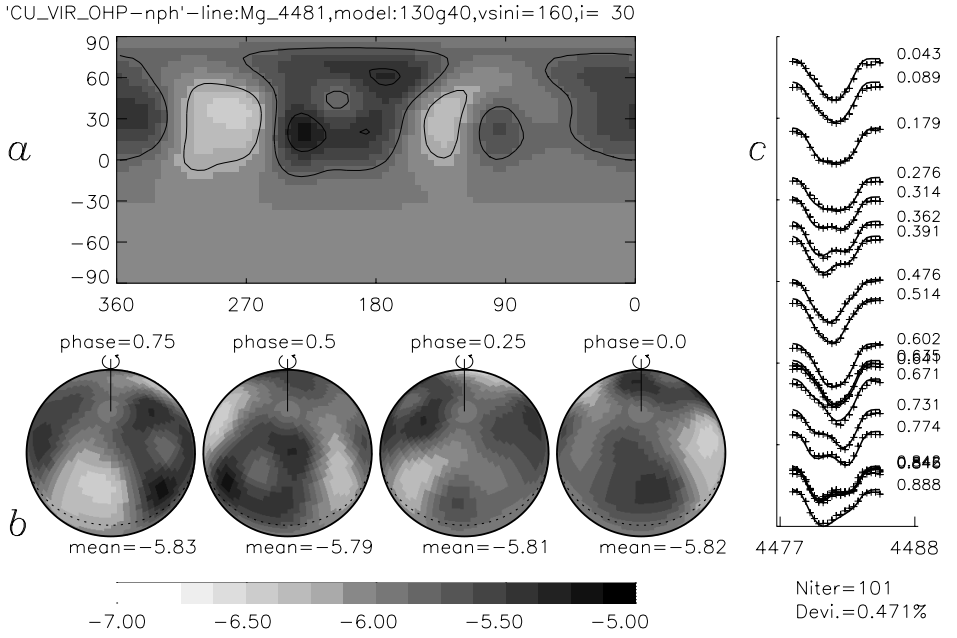

Fig. 3a–c. The map of CU Vir obtained from the strong magnesium 4481 Å blend. For details see Fig. 2.

to–noise ratios of these spectra were much poorer than in our case they were able to resolve similar features for helium.

Silicon maps were published by Hatzes (1993, 1996, 1997), which all were obtained from the Si ii line at 6347 Å, and the maps are coded with only three gray levels. A region of clear silicon underabundance is present which was already identified by Goncharski et al. (1983) using the Si ii λ 3862 line.

5.2. Comparison with diffusion models

Helium: Assuming a global dipolar magnetic field geometry, the helium diffusion model for main sequence magnetic stars (Vauclair et al. 1991) predicts that this element should be underabundant at the magnetic equator where the field lines are horizontal, but that it can be "normal" at the magnetic poles. They argue that gravitational settling dominates the radiative acceleration as well as thermal diffusion, which causes helium to sink in the atmosphere below the line–forming region. In addition, the suggested mass loss for heavier elements at the magnetic poles (polar wind) should be suppressed at the magnetic equator which significantly reduces the rate of the vertical diffusion. When metals are removed by stellar wind at the magnetic poles the remaining material, e.g. helium, is lifted upwards against the gravitational forces. The helium distribution we obtained is in agreement with this concept, as the location of the helium spot (see Fig. 2) coincides with a magnetic pole of CU Vir, which

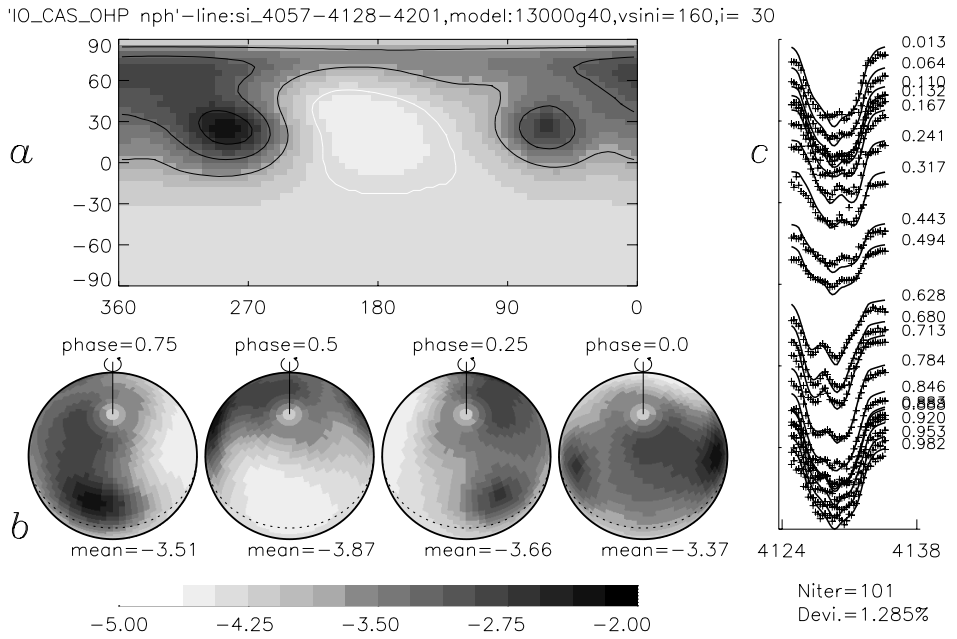

Fig. 4a–c. The silicon map of CU Vir obtained from the 3 different line blends of Si ii (4057 Å, 4128–4130 Å, and 4201 Å). For details see Fig. 2.

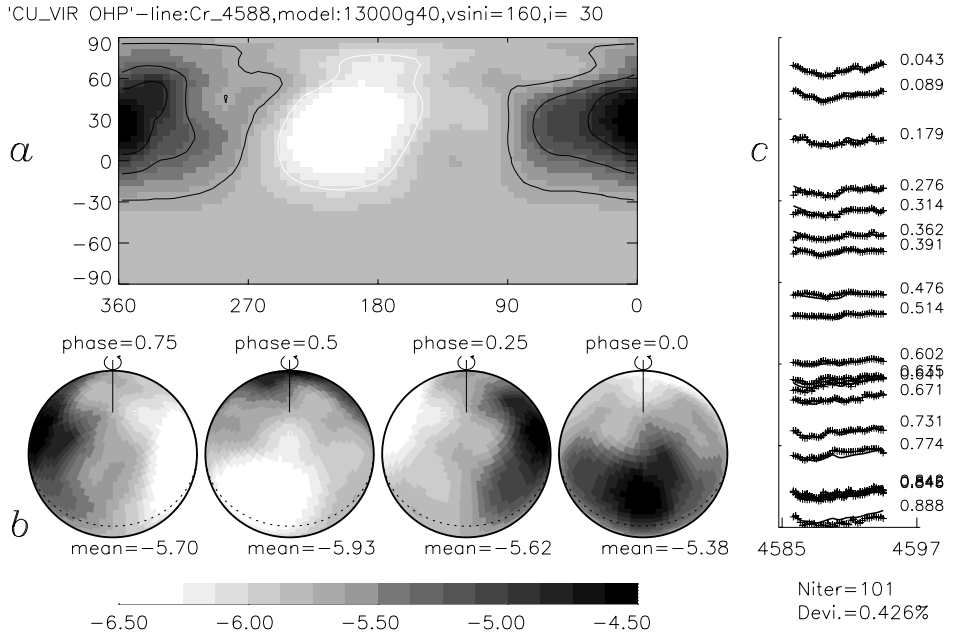

Fig. 5a–c. The chromium map of CU Vir obtained from 9 Cr ii lines in the region from 4586 Å to 4594 Å. For details see Fig. 2.

is confirmed indeed by the magnetic field curve presented by Pyper et al. (1998).

Silicon and iron-peak elements: Michaud et al. (1981) modeled diffusion in magnetic Ap–Bp stars. They found silicon to accumulate where the field lines are parallel to the stellar surface and to deplete at the poles where the field lines are mainly radially oriented. The same result was derived by Vauclair et al. (1979) and Alecian & Vauclair (1981). Megessier (1984) investigated the migration of silicon along magnetic field lines penetrating the atmosphere. Especially the latter work predicts Si to migrate in magnetic Ap star atmospheres in about 10^8 years from the equatorial region, where it surfaces, to the polar region. This model should be valid in the $T_{\rm eff}$ range from 12000 to 14000 K and for dipolar magnetic fields of up to 10^5 Gauss.

Babel (1992, 1995) investigated the abundance distribution of selected metals in the presence of a weak stellar wind, respectively mass loss rates of the order of 10^{-13} to 10^{-15} $M_\odot$, and assuming a particle outflow which is locally constrained by the magnetic field orientation in the sense that a significant metal wind exits only at the polar caps. Such a model was applied to the well studied cool magnetic Ap star 53 Cam and it could indeed reproduce the observed line profile variations. The behavior of lighter elements was not included in his study, but this would be definitely desirable for hotter Ap stars, like CU Vir.

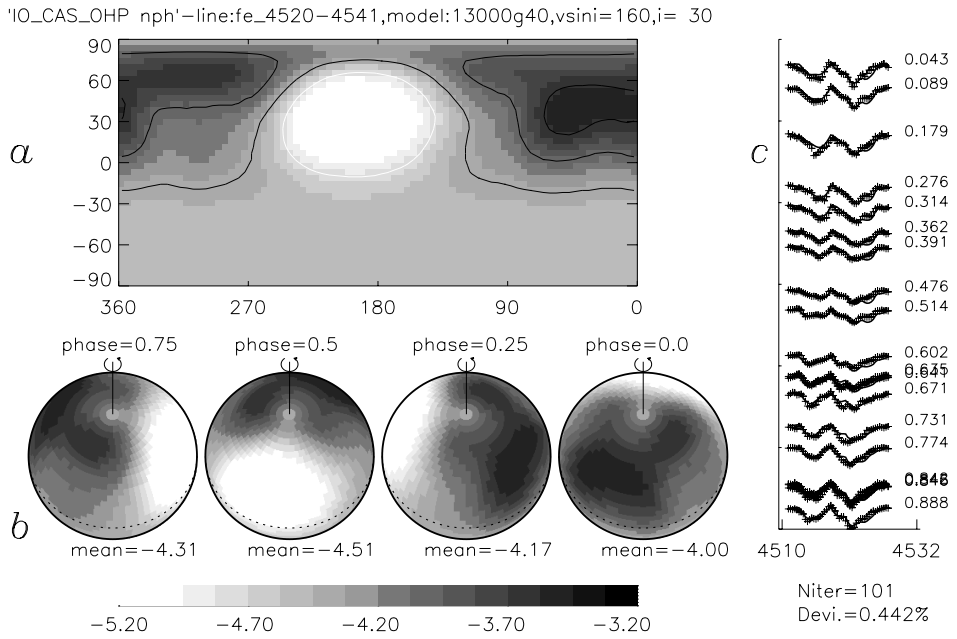

Fig. 6a–c. The iron surface distribution of CU Vir obtained from 11 Fe ii lines at 4520 Å and 4541 Å. For details see Fig. 2.

We found a similar surface distribution for silicon, chromium and iron, but clear differences for helium and magnesium. The conspicuous silicon enhancement in a "ring" centered on the magnetic pole (if the latter is marked indeed by the helium spot) seems to be correlated with magnetic field lines which are not much inclined to the surface, assuming a probably oversimplified dipolar magnetic field geometry. Considering Mégessier's (1984) analysis, the silicon diffusion mechanism has not been in effect long enough to transport this element to the polar region, which is consistent with the position of this star on the main sequence. Our results for Si, Cr and Fe are in agreement with the weak polar wind model proposed by Babel.

The magnesium distribution reflects an "intermediate" behavior compared to the other elements. It surrounds the helium spot (magnetic pole) but is also present in areas where Si, Cr and Fe are concentrated. Furthermore, Mg on average is depleted by a factor of 30. No theoretical investigation on the diffusion characteristics of this element could be found in the literature. A recent study of the magnesium abundance in B-type normal and in CP stars by Leone at al. (1997) showed that this element tends to be more underabundant in hot Ap stars, if the peculiarity and magnetic field strength increases. In contrast, for helium rich stars Mg may be even overabundant.

5.3. The magnetic field geometry

Recently, Hatzes (1997) investigated a decentered dipolar magnetic field configuration which fits the effective magnetic field measurements published by Borra and Landstreet (1980) within the error bars. This simple model is supported by the silicon map he obtained, showing a depletion region at one magnetic pole. But certainly more complex magnetic field structures, which were indicated for example by Leroy et al. (1995) for other Ap stars and which are based on linear polarimetry should be also considered. The helium spot we obtained (Fig. 2) allows one to locate one magnetic pole on CU Vir with high confidence, assuming the validity of Vauclair et al.'s (1991) model. The pole is located at +30° stellar latitude which results in an obliquity angle β of about 60° and which is within the error range for the 70° determined by Hatzes. Furthermore, assuming a centered dipole, the second pole should be at -30° latitude and hence cannot be observed directly due to the low inclination angle. Nevertheless, there is an indication for a marginal He abundance increase close to the equator at 20° longitude (Fig. 2), which is located exactly opposite to the visible pole. The distribution of silicon, chromium and iron supports the model, because these elements accumulate where the magnetic field lines are mainly horizontal and they deplete at the pole where the field lines basically are vertical to the stellar surface.

5.4. Hδ line variations

Balmer line variability of CU Vir was first reported by Ryabchikova (1972). Weiss et al. (1976) found a significant variation of the β-index out of phase with $uvby$ light curves which was corroborated by Hardorp & Megessier (1977). Musielok & Madej (1988) confirmed this phase shift and found a similar behavior for 56 Ari, which is also a B9p star and with a very short rotation period. As an explanation the latter authors proposed electron pressure gradients in combination with strongly magnetized plasma which generate electric currents and as a consequence influence the hydrostatic and radiative equilibrium in the stellar atmosphere.

Considering the depth dependency of this effect, phase shifts between magnetic field, hydrogen line widths and photometric light curves could be explained. Qualitatively, this model is supported by the Hδ equivalent widths variations (Fig. 1a) which we found to be slighgtly out of phase with helium (Fig. 2d). Fur-

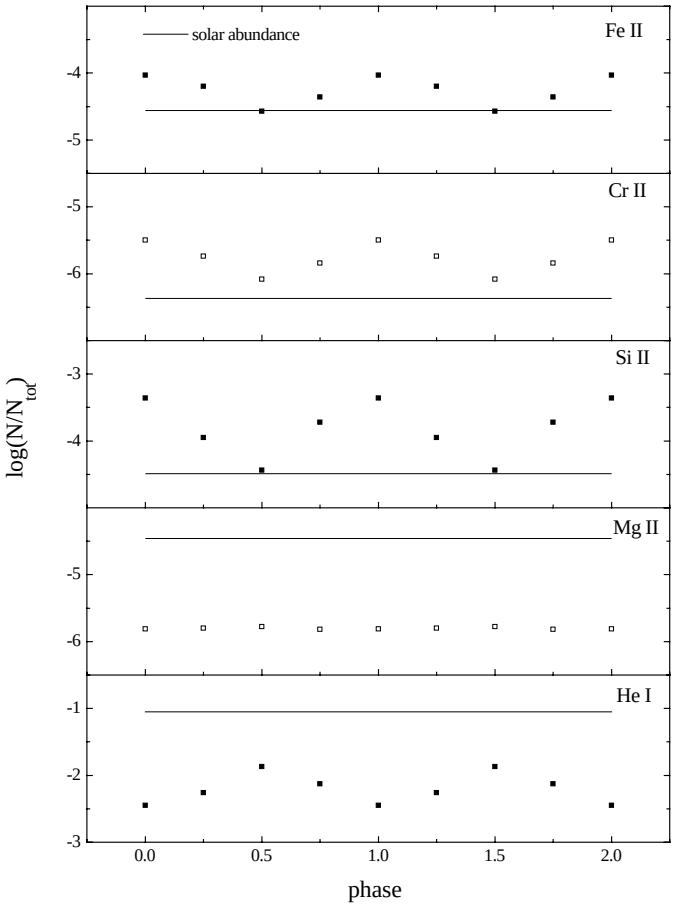

Fig. 7. The disk averaged abundances for He, Mg, Si, Cr and Fe. For each element the solid horizontal line refers to the solar abundance value.

thermore, we were able to fit the Hδ line even at extreme phases with models of the same $T_{\rm eff}$ = 12500 K$\pm$200 K and a $\log\ g$ of 3.9$\pm$0.1 for the phase of equivalent width minimum, but a $\log\ g$ of 4.2$\pm$0.1 is needed for the maximum. Fig. 8 illustrates the excellent Hδ line profile fits we obtained in the core as well as in the unblended part of the wings with the mentioned model parameters.

A $\log\ g$ difference between the two extreme phases, however, can also be expected due to the rather extreme He abundance of log(He/H) = -1.1 within the spot and of -2.4 outside. At about phase 0.0 more hydrogen atoms per gram contribute to the continuous absorption than at phase 0.5 where absorption is strongly reduced by about twenty times more helium atoms in the same mass unit, but the latter are not contributing to the continuous absorption at this temperature. As a consequence, a smaller absorption coefficient κ has the same effect on the relation between pressure and optical depth than a larger g, because only the quantity g/κ enters the hydrostatic equation. Transforming the derived He abundance variations into gravity effects results in a $\log\ g$ difference of 0.14 which is already half of the value determined by us from the Hγ profiles. Considering the errors for the $\log\ g$ determination, the changes in the helium abundance could even produce the full $\log\ g$ difference. However, it should be remembered that this mechanism cannot produce the observed phase shift between extreme values of $\log\ g$ and the He abundance. Fortunately, at least at the present level of sophistication, these second order problems with stellar atmospheres do not influence the structure of Doppler images (Kuschnig 1998) which are the main subjects of the present paper.

6. Conclusions

Based on the abundance distribution of the five elements He, Mg, Si, Cr, and Fe, which we obtained with a Doppler Imaging technique, and on the Hδ line variations we draw the following conclusions:

- the surface distributions of Si, Cr and Fe are very similar and *on average* all these elements are enhanced relative to the sun. The distribution, however, is not homogeneous and most of the elements are less abundant in areas where He is enriched, and vice versa. Magnesium behaves distinctly different, as it has a rather homogeneous distribution, and on average is depleted relative to the sun. One ring like feature seems to surround the helium spot, but Mg is also present in the Si, Cr and Fe enriched areas.
- based on the theoretical investigations of helium diffusion in the atmosphere of magnetic stars (Vauclair et al. 1991) and assuming a simple dipolar magnetic field geometry the observed helium spot should indicate the location of one of the magnetic poles of CU Vir. A decentered dipole model was investigated by Hatzes, but his model does not change our conclusions. The distribution of silicon is consistent with the results presented by Mégessier (1984) for stars at the main sequence. The chromium and iron maps can be understood in the framework of the weak polar wind model introduced by Babel (1992) which results in metal depletion at the polar caps. The magnesium distribution presently can not be compared with the predictions of the diffusion theory as the calculations for this element are still missing.
- we found the Hδ line variations to be in phase with the magnetic field and we can fit the Hδ line profiles based on models with $T_{\rm eff}$ = 12500 K, $\log\ g$ = 3.9 (at minimum line intensity), and $\log\ g$ = 4.2 (at maximum line intensity). This result indicates, at least empirically, that the atmospheric structure of CU Vir is quite inhomogeneous. Furthermore, the high rotational velocity of CU Vir in combination with the magnetic field may result in a substantial deviation from a spherical symmetry of this star.

The future investigations of CU Vir will be focused on mapping of other elements with different diffusion characteristics, in particular of the CNO group, calcium and rare earth elements. These new observations should be supplemented by simultaneous magnetic field and photometric measurements in order to exploit the full information content of spectroscopy and to reduce ambiguities due to insufficiently known rotation phases.

From the theoretical point of view, more detailed investigations of the diffusion and mass loss effects in the atmosphere

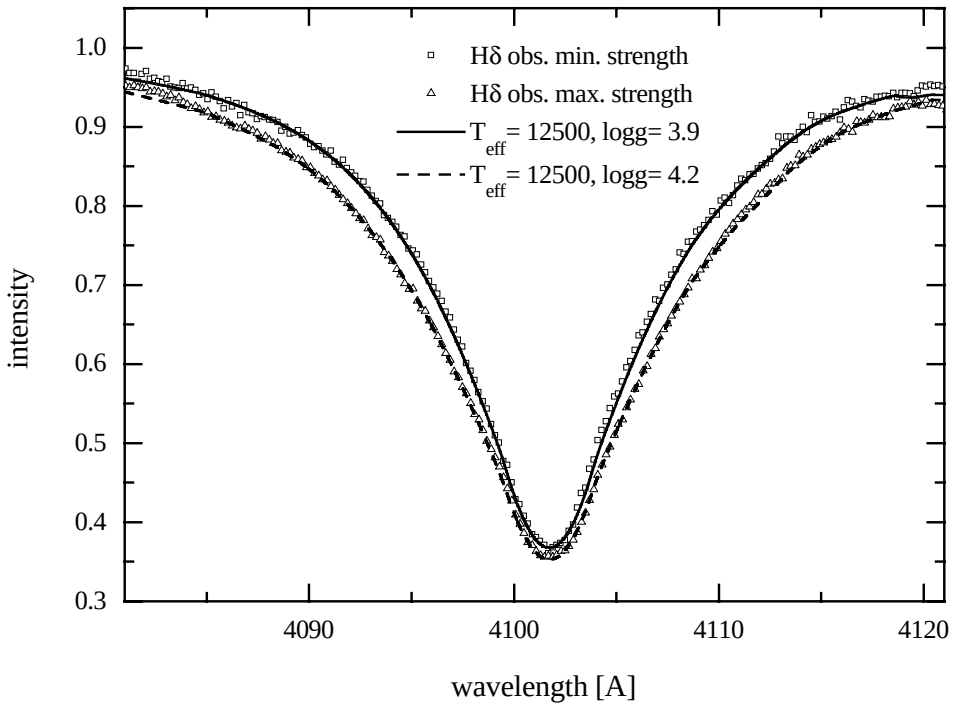

Fig. 8. Hδ line profiles at phases of maximum and minimum line strength, compared with the calculations.

of stars like CU Vir definitely are needed. Such models should account for global atmospheric inhomogeneities which are indicated by the strong Balmer line variations for CU Vir. Furthermore, the rather abrupt change in the rotation period poses a serious challenge to the astrophysical understanding of this interesting star.

Acknowledgements. This research was done within the working group *Asteroseismology-AMS* and supported by the Fonds zur Förderung der wissenschaftlichen Forschung (project *S 7303-AST*). The calculations were performed with a DEC AXP-3000/600, funded through a DEC-EERP project (STARPULS). T.R. thanks the Russian Federal Research Foundation for financial support through grant No.95-02-06359.

References

Adelman S.J., Dukes R.J. Jr., Pyper D.M., 1992, AJ 104, 314
Alecian G., Vauclair S., 1981, A&A 101, 16
Babel J., 1992, A&A 258, 449
Babel J., 1995, A&A 301, 823
Blanco C., Catalano F., 1971, A&A 76, 630
Borra E.F., Landstreet J.D., 1980, ApJS 42, 421
Goncharski A.V., Ryabchikova T.A., Stepanov V.V., Khokhlova V.L., Yagola A.G., 1983, Sov. Astron. 27, 49
Hardorp J., Megessier C., 1977, A&A 61, 411
Hatzes A.P., 1993, In: Dworetsky M.M., et al. (eds.) Peculiar versus Normal Phenomena in A-type and Related Stars. IAU Coll. 138, ASP Conf. Ser. 44, p. 258
Hatzes A.P., 1996, In: Strassmeier K.G., Linsky J.L. (eds.) Stellar Surface Structure. IAU Symp. 176, Kluewer, p. 305
Hatzes A.P., 1997, MNRAS 288, 153
Hiesberger F., Piskunov N.E., Bonsack W.K., et al., 1995, A&A 296, 473
Kurucz R.L., 1993, In: Dworetsky M.M., et al. (eds.) Peculiar versus Normal Phenomena in A-type and Related Stars. IAU Coll. 138, ASP Conf. Ser. 44, p. 87
Kuschnig R., 1998, Thesis, University Vienna
Kuschnig R., Ryabchikova T.A., Piskunov N.E., Weiss W.W., 1996, In: Strassmeier K.G. (ed.) Stellar Surface Structure. IAU Symp. 176, Poster Procceedings, p. 135
Leone F., Catalano F.A., Malaroda S., 1997, A&A 325, 1125
Leroy J.L., Landolfi M., Landi Degl'Innocenti M., et al., 1995, A&A 301, 797
Michaud G., 1970, ApJ 160 640
Michaud G., Megessier C., Charland Y., 1981, A&A 103, 244
Megessier C., 1984, A&A 138, 267
Musielok B., Madej J., 1988, A&A 202, 143
Piskunov N.E., Kupka F., Ryabchikova T.E., et al., 1995, AA&S 112, 525
Piskunov N.E., Rice J.B., 1993, PASP 105, 1415
Preston G.W., 1974, ARA&A 12, 257
Pyper D., Ryabchikova T.A., Malanushenko V., et al., 1998, A&A 339, 822
Rice J.B., 1996, In: Strassmeier K.G., Linsky J.L. (eds.) Stellar Surface Structure. IAU Symp. 176, Kluewer, p. 305
Ryabchikova T.A., 1972, Izv. Krymsk. Astrofiz. Obs. 45, 146
Smirnov O.M., Piskunov N., Astronomical Image Processing on the PC with PCIPS. 1994, In: Crabtree D.R., Hanish R.J., Barnes j. (eds.) Astronomical Data Analysis Software And Systems III, Victoria 1993, Astron. Soc. of Pacific, Conference series Vol. 61, p. 245
Stepien K., 1998, A&A 337, 754
Stibbs D.W.N., 1950, MNRAS 110, 410
Vauclair S., Hardorp J., Peterson D., 1979, ApJ 227, 526
Vauclair S., Dolez N., Gough D.O., 1991, A&A
Weiss W.W., Albrecht R., Wieder R., 1976, A&A 47, 423